

# Velocity Slip and Temperature Jump in Hypersonic Aerothermodynamics

Andrew J. Lofthouse\*, Leonard C. Scalabrin\* and Iain D. Boyd†

*Department of Aerospace Engineering, University of Michigan, Ann Arbor, 48109*

Hypersonic vehicles experience different flow regimes during flight due to changes in atmospheric density. Computational Fluid Dynamics (CFD), while relatively computationally inexpensive, is not physically accurate in areas of highly non-equilibrium flows. The direct simulation Monte Carlo (DSMC) method, while physically accurate for all flow regimes, is relatively computationally expensive. In a continuing effort to understand the performance of CFD and DSMC in hypersonic flows, the current study investigates the effect of continuum breakdown on surface aerothermodynamic properties (pressure, shear stress and heat transfer rate) of a cylinder in Mach 10 and Mach 25 flows of argon gas for several different flow regimes, from the continuum to a rarefied gas. Several different velocity slip and temperature jump boundary conditions are examined for use with the CFD method. CFD and DSMC solutions are obtained at each condition. Total drag and peak heat transfer rate predictions by CFD remains within about 6% of the DSMC predictions for all regimes considered, with the generalized slip condition proposed by Gökçen giving the best results.

## Nomenclature

|       |                           |
|-------|---------------------------|
| $A$   | Constant                  |
| $d$   | Molecular diameter        |
| $k$   | Boltzmann constant        |
| $L$   | Characteristic length     |
| $m$   | Mass of one molecule      |
| $q$   | Heat transfer rate        |
| $T$   | Translational Temperature |
| $T_j$ | Temperature jump          |
| $T_w$ | Wall temperature          |
| $u_x$ | Velocity in x-direction   |
| $V_n$ | Velocity normal to wall   |
| $V_p$ | Velocity parallel to wall |
| $V_s$ | Slip velocity             |
| $p$   | Pressure                  |

### *Symbols*

|           |                                    |
|-----------|------------------------------------|
| $\lambda$ | Mean free path                     |
| $\mu$     | Coefficient of viscosity           |
| $\omega$  | VHS temperature exponent           |
| $\rho$    | Mass density                       |
| $\sigma$  | Momentum accommodation coefficient |
| $\tau$    | Shear stress parallel to wall      |

---

\*Graduate Student, Member AIAA.

†Professor, Associate Fellow AIAA

“The views expressed in this paper are those of the author and do not reflect the official policy or position of the United States Air Force, Department of Defense, or the U.S. Government”

## I. Introduction

The design of hypersonic vehicles requires accurate prediction of the surface properties while in flight. These quantities are typically the heat flux, pressure and shear stress. These variables govern not only the aerodynamic performance of the vehicle, but also determine the selection and sizing of the thermal protection system (TPS), which protects the vehicle from the entry environment. During its trajectory through an atmosphere, a hypersonic vehicle will experience vastly different flow regimes because the atmosphere's density varies as a function of altitude. Reproduction of these varied flow conditions in ground-based laboratory facilities is both expensive and technically challenging. Hence, there is an extremely important role for computational models in the development of hypersonic vehicles.

At low altitudes, the atmospheric density is relatively high, and flows around hypersonic vehicles should be simulated using traditional Computational Fluid Dynamics (CFD) by solving either the Euler or preferably the Navier-Stokes (NS) equations. This is the continuum regime characterized by very large Reynolds numbers and very low Knudsen numbers, where the Knudsen number is defined in Eq. 1.

$$\text{Kn} = \frac{\lambda}{L} \propto \frac{1}{\rho L} \quad (1)$$

At very high altitudes, at the edge of the atmosphere, the density is low such that there are very few collisions between the molecules and atoms in the flow around the vehicle. This is the rarefied flow regime and can be computed using the direct simulation Monte Carlo (DSMC) method.<sup>1</sup> Generally speaking, CFD methods for solving the NS equations are about an order of magnitude faster than the DSMC method. However, the lack of collisions makes the physics of the NS equations invalid in rarefied regimes, which is characterized by a large Knudsen number. On a blunt body, a high-density fore-body flow can create a rarefied flow in the wake of the vehicle. In principle, the DSMC method can be applied to any dilute gas flow, but becomes prohibitively expensive for Knudsen numbers less than 0.001. Thus, it is attractive to find ways to increase the validity of CFD methods beyond the continuum regime.

One way to improve CFD modeling in the transition regime, that is, for lower density flows beyond the continuum regime and before the free molecular regime, is by replacing the typical no-slip boundary conditions with slip velocity and temperature jump boundary conditions. The addition of slip boundary conditions will not, however, eliminate all source of errors when using continuum methods for flows with large amounts of non-equilibrium. For instance, in more rarefied flows, the pressure tensor ceases to be isotropic, a key assumption in the derivation of the continuum equations.

The areas of the flow where the continuum hypothesis breaks down (or equivalently, where the flow is no longer in local thermodynamic equilibrium), can be quantified by the use of a continuum breakdown parameter. While there have been several breakdown parameters presented in the literature,<sup>2-5</sup> the one that appears to be most appropriate for hypersonic compressible flows is the gradient-length local (GLL) Knudsen number<sup>6,7</sup>

$$\text{Kn}_{\text{GLL}} = \frac{\lambda}{Q} \left| \frac{dQ}{dl} \right| \quad (2)$$

where the derivative is taken in the direction of the maximum gradient, and  $Q$  is some quantity of interest such as density, pressure, temperature or velocity magnitude. When calculating  $\text{Kn}_{\text{GLL}}$  based on velocity magnitude, the gradient is normalized by the maximum of the local velocity magnitude and the local speed of sound. It is generally assumed that continuum breakdown occurs whenever  $\text{Kn}_{\text{GLL}}$  (based on the CFD solution) is greater than 0.05.

Previous work<sup>8</sup> sought to quantify the errors in CFD predictions of surface properties of a hypersonic blunt body by comparing those solutions with DSMC solutions for a variety of flows in the transitional regime. The maximum  $\text{Kn}_{\text{GLL}}$  was also computed in each case to determine the effect of continuum breakdown on the surface properties. The cases considered were limited to a Mach 10 flow of argon. The previous CFD solutions were obtained with no-slip boundary conditions imposed at the wall. As would be expected when only considering a simple gas, the results indicated that the inclusion of velocity slip and temperature jump boundary conditions would improve the agreement between the DSMC and CFD conditions.

The current work builds on these results with the main objective being to quantify the improvement in agreement between the DSMC solutions and the CFD solutions with the inclusion of slip boundary conditions. Additional cases of a Mach 25 flow are also computed to determine any effects of continuum breakdown at higher velocities on the surface properties.

This paper will first briefly describe the simulation procedures used, including some background of the computational models. Several slip boundary conditions are then evaluated. It will then discuss general flow field and surface property results predicted by the models in several different flow regimes, from the continuum to a rarefied gas. Finally, some conclusions are presented.

## II. Background and Simulation Procedure

This investigation continues previous work that considered a hypersonic flow of argon over a two-dimensional, 12-inch diameter cylinder, as shown in Figure 1. Two different free stream velocities are used that correspond to Mach 10 and Mach 25 flows ( $U_\infty = 2624.1$  m/s and 6585 m/s, respectively). The wall temperature is held constant at 500 K (Mach 10) and 1500 K (Mach 25). The free stream density of the flow is varied such that several different regimes are considered, from the continuum through the transitional to the rarefied regime, as shown in Table 1. Knudsen numbers are calculated based on freestream conditions and the cylinder diameter, using the hard-sphere model for the mean free path calculation. Surface and flow field properties for this flow are presented from two different computational approaches.

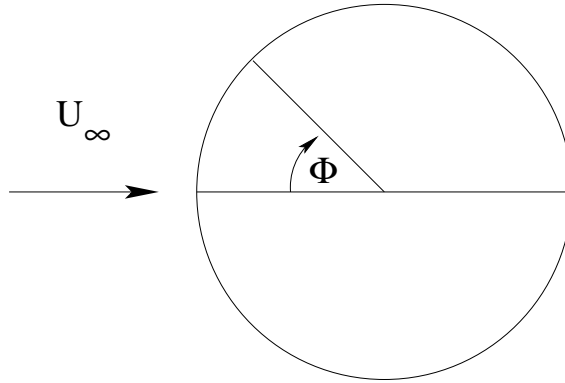


Figure 1. Geometry definition.

First, CFD results are obtained through solution of the Navier-Stokes equations. The CFD results are obtained using the Michigan Aerothermodynamic Navier-Stokes (LeMANS) code, developed at the University of Michigan for the simulation of hypersonic reacting flow-fields.<sup>9,10</sup> LeMANS is a general 2D/3D, parallel, unstructured, finite-volume CFD code capable of simulating gases in thermal and chemical non-equilibrium. All LeMANS solutions are generated assuming an isothermal wall at 500 K (Mach 10) and 1500 K (Mach 25). Different boundary conditions, including no-slip and slip velocity and temperature jump are enforced. These will be discussed in more detail below. In each case, a grid independence study was conducted to determine the final mesh resolution used.

Second, DSMC results are provided from the MONACO code<sup>11</sup> for the same flow conditions. MONACO is a general 2D/3D, parallel, unstructured mesh DSMC code that has been applied to many hypersonic, rarefied flows.<sup>12</sup> All MONACO solutions are generated using a fixed wall temperature at 500 K and 1500 K. Bird's variable hard sphere model is used.<sup>1</sup> In general, the mesh used for the final solution for each case is adapted from previous solutions such that each cell size is on the order of a mean free path. The exceptions are the  $Kn = 0.002$ , where the cell size is approximately four times the mean free path, and the  $Kn = 0.01$ , where the cell sizes near the surface are on the order of two mean free paths in size. In these cases the subcell method is used to select particles for collisions<sup>1</sup> to ensure physical accuracy.

The variable hard sphere (VHS) parameters used in the DSMC computations are equivalent to those used in the previous work (the temperature exponent,  $\omega$ , is 0.734 with a reference diameter of  $3.595 \times 10^{-10}$  m at

Table 1. Flow regimes considered.

| $Kn_\infty^*$ | Mass Density<br>(kg/m <sup>3</sup> ) | Number Density<br>(particles/m <sup>3</sup> ) |
|---------------|--------------------------------------|-----------------------------------------------|
| 0.002         | $1.408 \times 10^{-4}$               | $2.124 \times 10^{21}$                        |
| 0.01          | $2.818 \times 10^{-5}$               | $4.247 \times 10^{20}$                        |
| 0.05          | $5.636 \times 10^{-6}$               | $8.494 \times 10^{19}$                        |
| 0.25          | $1.127 \times 10^{-6}$               | $1.699 \times 10^{19}$                        |

\* Based on hard-sphere mean free path.

a reference temperature of 1000 K). The viscosity and thermal conductivity of pure argon in the CFD code are computed to exactly correspond to the VHS model, according to Eqs. 3 and 4.<sup>13</sup>

$$\mu = \mu_{ref} \left( \frac{T}{T_{ref}} \right)^\omega \quad (3)$$

$$\mu_{ref} = \frac{15\sqrt{\pi mkT_{ref}}}{2\pi d_{ref}^2 (5 - 2\omega)(7 - 2\omega)} \quad (4)$$

Some computational details are given in Table 2. It should be noted here that both MONACO and LeMANS are research codes. Additional improvements to DSMC codes have been proposed<sup>14</sup> that may reduce the computational expense of the DSMC calculations. The LeMANS code is very new and has not been extensively optimized for performance. Also, the CFD cases cited in Table 2 correspond to the Type 2 slip condition (discussed below) which had the slowest convergence rate. Additional work will most likely yield much better computational efficiency.

**Table 2. DSMC and CFD computational details.**

### Mach 10

| Kn <sub>∞</sub> | DSMC    |                       |            |      | CFD    |            |      |
|-----------------|---------|-----------------------|------------|------|--------|------------|------|
|                 | Cells   | Particles             | Time Steps | CPUs | Cells  | Iterations | CPUs |
| 0.002           | 394,250 | 287.0×10 <sup>6</sup> | 1,050,000  | 128  | 80,000 | 60,000     | 8    |
| 0.01            | 68,497  | 26.8×10 <sup>6</sup>  | 430,000    | 32   | 40,000 | 55,000     | 8    |
| 0.05            | 18,818  | 7.1×10 <sup>6</sup>   | 430,000    | 32   | 40,000 | 87,000     | 8    |
| 0.25            | 24,452  | 8.2×10 <sup>6</sup>   | 290,000    | 32   | 40,000 | 90,000     | 8    |

### Mach 25

| Kn <sub>∞</sub> | DSMC    |                       |            |      | CFD    |            |      |
|-----------------|---------|-----------------------|------------|------|--------|------------|------|
|                 | Cells   | Particles             | Time Steps | CPUs | Cells  | Iterations | CPUs |
| 0.002           | 121,063 | 142.0×10 <sup>6</sup> | 1,400,000  | 128  | 80,000 | 42,000     | 8    |
| 0.01            | 87,364  | 32.6×10 <sup>6</sup>  | 460,000    | 32   | 40,000 | 50,000     | 8    |
| 0.05            | 33,268  | 18.7×10 <sup>6</sup>  | 450,000    | 32   | 40,000 | 65,000     | 8    |
| 0.25            | 14,006  | 9.7×10 <sup>6</sup>   | 300,000    | 32   | 40,000 | 67,000     | 8    |

## II.A. Slip Boundary Conditions

This section discusses several different types of slip boundary condition and their implementation in the LeMANS code.

The slip boundary condition was first derived by Maxwell for a flat plat. The expression he derived for the slip velocity is shown in Eq. 5,<sup>15</sup> where wall coordinates are used ( $n$  is normal to the wall and  $x$  is parallel to the wall).

$$V_s = A \left( \frac{2 - \sigma}{\sigma} \right) \lambda \frac{\partial u_x}{\partial n} + \frac{3}{4} \frac{\mu}{\rho T} \frac{\partial T}{\partial x} \quad (5)$$

For an isothermal wall, the temperature gradient can be neglected, giving the boundary condition in its simplest form in Eq. 6.

$$V_s = A \left( \frac{2 - \sigma}{\sigma} \right) \lambda \frac{\partial u_x}{\partial n} \Big|_0 \quad (6)$$

The mean free path,  $\lambda$ , is calculated from typical gas flow properties as shown in Eq. 7.<sup>16</sup>

$$\lambda = \frac{2\mu}{\rho c} = \frac{\mu}{\rho} \sqrt{\frac{\pi}{2RT}} \quad (7)$$

The boundary condition for temperature jump is similar, seen in Eq. 8.<sup>17</sup>

$$T_0 - T_w = \frac{2 - \alpha}{\alpha} \frac{2\gamma}{(\gamma + 1) \text{Pr}} \lambda \left. \frac{\partial T}{\partial n} \right|_0 \quad (8)$$

The thermal accommodation coefficient,  $\alpha$ , can be assumed to be the same as the momentum accommodation coefficient,  $\sigma$ . In this case, the second and third terms on the right hand side can be combined and an equivalent mean free path adopted as

$$\lambda_T = \frac{4}{(\gamma + 1)} \frac{\kappa}{\rho \bar{c} C_v} = \frac{2}{(\gamma + 1)} \frac{\kappa}{\rho C_v} \sqrt{\frac{\pi}{2RT}} \quad (9)$$

to give the simpler form shown in Eq. 10.

$$T_0 - T_w = \frac{2 - \alpha}{\alpha} \lambda_T \left. \frac{\partial T}{\partial n} \right|_0 \quad (10)$$

The simple Maxwell slip conditions given by Eqs. 6 and 10 are implemented in LeMANS and referenced below as the Type 1 slip condition.

Throughout many years of research, the general form of the velocity slip has remained the same, while the difficulty is in determining the correct value for the constant,  $A$ , and the accommodation coefficients,  $\sigma$  and  $\alpha$ . Many times these coefficients are determined empirically, while other times they are calculated from relations based on kinetic theory.<sup>18</sup> The most detailed boundary conditions require knowledge *a priori* of a good non-equilibrium solution for the flow being considered. In effect, any change in  $A$  simply changes the value of the accommodation coefficient, which depends on the physical characteristics of the wall itself.<sup>19</sup> The current investigation seeks to find a good boundary condition that does not require *a priori* knowledge of any non-equilibrium solution, which would eliminate any advantage in using CFD over DSMC. Also, both the DSMC and CFD solutions are calculated assuming a fully diffuse wall, which corresponds to an accommodation coefficient of 1.

The previous, simple slip boundary conditions were derived for small Knudsen numbers. Gökçen<sup>16</sup> showed that, for large Knudsen numbers, these simple slip boundary conditions converge to different values than those predicted by free molecular flow. He then proposed the general slip boundary conditions given in Eq. 11.

$$\alpha_a (a_\lambda - a_w) = 2\lambda_a \left. \frac{\partial a}{\partial n} \right|_0 \quad (11)$$

Here,  $a$  is either velocity or temperature, and  $\lambda_a$  is given by either Eq. 7 or 9. For small Knudsen numbers, this expression reduces to Eqs. 6 and 10.<sup>17</sup> This slip condition is referenced in the results below as the Type 2 slip condition.

As mentioned previously, the original Maxwell slip boundary condition was derived for a flat plate. Lockerby *et al.*<sup>15</sup> showed that for a curved wall the proper boundary condition is given by Eq. 12. This is known as the extended slip boundary condition.

$$V_s = \left( \frac{2 - \sigma}{\sigma} \right) \lambda \left( \frac{\partial u_x}{\partial n} + \frac{\partial u_n}{\partial x} \right) + \frac{3}{4} \frac{\mu}{\rho T} \frac{\partial T}{\partial x} \quad (12)$$

This slip condition is not implemented in LeMANS at this time and is not considered further here.

The Navier-Stokes equations fail in at least two different areas as the flow becomes more rarefied. The first area, an assumption of no-slip flow, is corrected through the use of the slip boundary conditions. However, the N-S equations also assume that the shear stress varies linearly with the velocity gradient at the wall. Cercignani showed the form that the velocity profile in the Knudsen layer takes.<sup>20</sup>

Here there are two choices one can make concerning the boundary conditions; use the actual slip velocity in which case the flow field away from the wall will not be accurate, or use a fictitious slip velocity. The fictitious slip will not accurately predict the flow near the wall (and hence may adversely affect the accuracy of drag and heat transfer rates) but will be more accurate in the region away from the wall.

A correction to the velocity gradient is evaluated by Lockerby *et al.*<sup>20</sup> They proposed using a wall-function type of boundary condition for the velocity where the viscosity in the Knudsen layer is modified

as  $\mu = \mu\Psi^{-1}$  where  $\Psi$  is given in Eq. 13, derived from a curve-fit to Cercignani’s Knudsen layer velocity profile.

$$\Psi\left(\frac{n}{\lambda}\right) \approx 1 + \frac{7}{10}\left(1 + \frac{n}{\lambda}\right)^{-3} \quad (13)$$

This modification of the viscosity in the Knudsen layer is also used in connection with a simple slip boundary condition as given by Eq. 6 with  $A = \sqrt{2/\pi}$ . This approach is expected to allow the CFD method to accurately model the velocity profile in the Knudsen layer.

This new wall function has only been evaluated for isothermal flow conditions that are usually encountered in micro-flows. Although there will be some change to the heat transfer rate coefficient (based on a constant Prandtl number), there might be other changes necessary to give the correct temperature profile in the Knudsen layer for the non-isothermal, hypersonic flows considered here. Nevertheless, it is instructive to investigate the possible improvement this wall function might afford. This slip condition is implemented in LeMANS and is referenced as the Type 3 slip condition.

The traditional no-slip boundary conditions are referenced below as the Type 0 boundary conditions.

## II.B. Slip Quantities and DSMC

The Boltzmann Equation inherently includes slip boundary conditions; therefore, the DSMC method includes them as well. In MONACO, the slip velocity and temperature jump are calculated based on the particles that strike the surface, according to Eqs. 14 and 15, which are the relations used in Bird’s DSMC implementation, DS2V.<sup>21,22</sup>

$$V_s = \frac{\sum((m/V_n)V_p)}{\sum(m/V_n)} \quad (14)$$

$$T_j = \frac{\sum((m/V_n)(u^2 + v^2 + w^2)) - \sum(m/V_n)V_s^2}{3k\sum(1/V_n)} - T_w \quad (15)$$

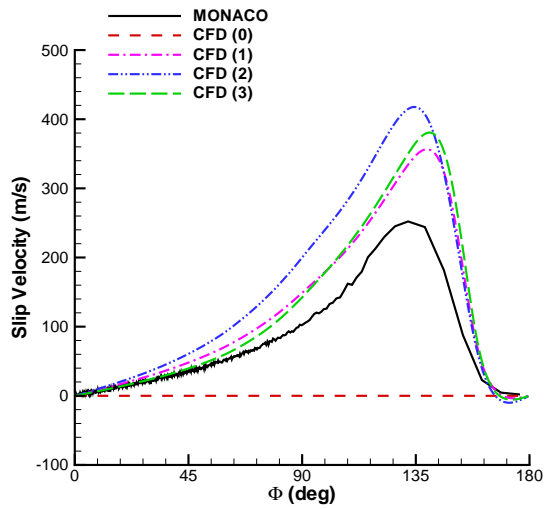
Comparison of MONACO and DS2V results show that the velocity slip and temperature jump results (using Eqs. 14 and 15) are nearly identical. This is not surprising considering that their implementations are identical. However, it is useful to compare the DSMC slip velocity and temperature jump to those obtained by the CFD slip conditions previously mentioned, in order to evaluate their relative merit. It appears, however, that the quantities computed according to Eqs. 14 and 15 may not be the best choice when comparing solutions. Figure 2 compares the CFD and DSMC data at the wall boundary for the Mach 10,  $\text{Kn} = 0.01$  case. The DSMC data is given by Eqs. 14 and 15 while the CFD data is given by the slip velocity and temperature jump according the equations in the previous section, depending on the case. Figure 3 compares the same case, but the data is extracted from the field solution  $5 \times 10^{-7}$  m from the surface of the cylinder, which is well within the Knudsen layer. Although Figure 2 suggests that the CFD solution predicts a higher velocity slip and temperature jump (and the temperature jump does not even follow the same general trend), Figure 3 suggests that the agreement is actually much closer, especially for the Type 2 boundary condition. Therefore, it appears that data extracted from the field data might be more appropriate to compare than the actual boundary data.

## III. Results

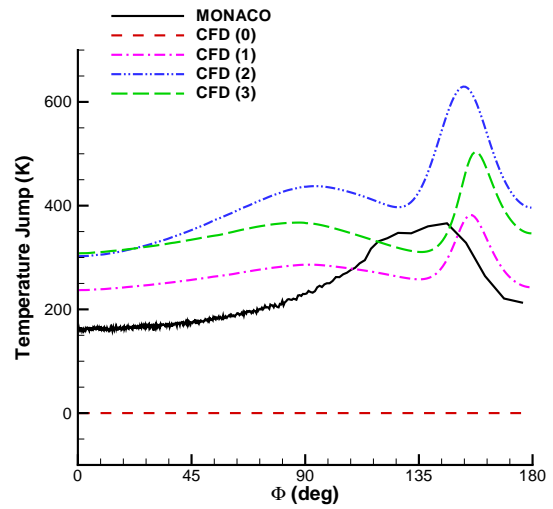
This investigation seeks to quantify the differences in the surface properties of a cylinder in a hypersonic flow by comparing CFD and DSMC predictions for total drag and peak heat transfer. Additionally, the overall flow features, such as the temperature field, are compared, as well as the surface distributions of pressure, shear stress and heat transfer.

Tables 3 and 4 compare the total drag and the peak heat transfer rates predicted by both computational methods. Here, the peak heat transfer rate is obtained by averaging over the surface area within one degree of the stagnation point. For CFD, these quantities are calculated for each of the different boundary conditions implemented, with Type 0 being the no-slip condition.

It is clear that the slip boundary conditions improve the agreement between the two simulation methods. While the difference in total drag is as high as 23.6% and 32.0% for the no-slip condition, the Type 2 slip boundary condition shows the best agreement, with the difference exceeding 5% only for the  $\text{Kn} = 0.25$  case.

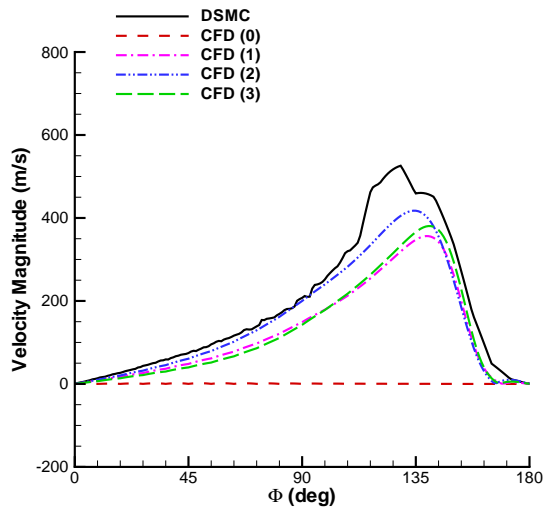


(a) Velocity Slip

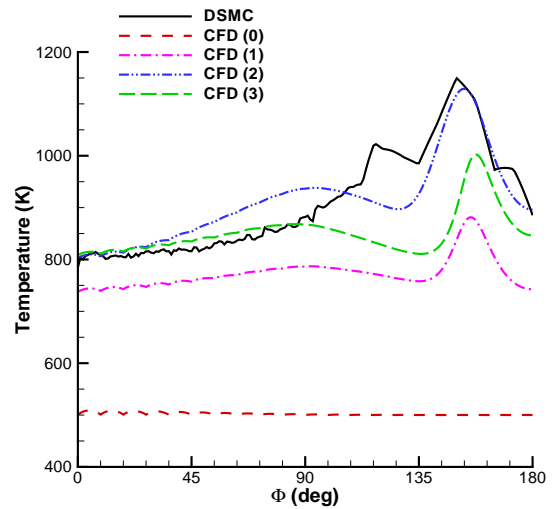


(b) Temperature Jump

Figure 2. Comparison of flow properties at the wall for CFD and DSMC using slip boundary conditions (CFD) and Eqs. 14 and 15 (DSMC). The DSMC properties are significantly different from all the CFD solutions.



(a) Velocity Magnitude



(b) Temperature

Figure 3. Comparison of flow properties for CFD and DSMC by extracting data from the field properties  $5 \times 10^{-7}$  m from the wall. Agreement between the two methods is better.

Similar trends are noted for the peak heat transfer rate, with a nearly 40% difference for the no-slip CFD solution, while the Type 2 slip solution remains near 1% or less for most of the cases and only exceeds 5% for the  $Kn = 0.25$  case at Mach 25.

There is also a slight improvement in drag and heat flux agreement between the Type 1 and Type 3 boundary conditions, where the only difference in the two boundary conditions is the inclusion in the Type 3 of the viscosity correction function within the Knudsen layer. This improvement is not as great as that achieved with the Type 2 boundary condition, but it might hint that the Type 2 condition could be improved with the addition of the viscosity correction in the Knudsen layer.

Since the Type 2 condition shows the best agreement with the DSMC solutions, the CFD temperature field results shown below are taken from the Type 2 CFD case.

**Table 3. Total drag.**

**Mach 10**

| $Kn_\infty$ | Drag/Length [N/m] (% Difference) |               |               |               |              |
|-------------|----------------------------------|---------------|---------------|---------------|--------------|
|             | DSMC                             | CFD (0)       | CFD (1)       | CFD (2)       | CFD (3)      |
| 0.002       | 187.6                            | 187.5 (-0.1%) | 187.4 (-0.1%) | 187.4 (-0.1%) | 187.6 (0.0%) |
| 0.01        | 40.02                            | 40.32 (0.8%)  | 40.19 (0.4%)  | 40.16 (0.4%)  | 40.27 (0.6%) |
| 0.05        | 8.900                            | 9.416 (5.8%)  | 9.122 (2.5%)  | 8.863 (-0.4%) | 9.078 (2.0%) |
| 0.25        | 2.092                            | 2.585 (23.6%) | 2.301 (10.0%) | 1.982 (-5.2%) | 2.253 (7.7%) |

**Mach 25**

| $Kn_\infty$ | Drag/Length [N/m] (% Difference) |               |               |               |               |
|-------------|----------------------------------|---------------|---------------|---------------|---------------|
|             | DSMC                             | CFD (0)       | CFD (1)       | CFD (2)       | CFD (3)       |
| 0.002       | 1,171                            | 1,176 (0.4%)  | 1,176 (0.4%)  | 1,176 (0.4%)  | 1,177 (0.5%)  |
| 0.01        | 250.8                            | 255.3 (1.8%)  | 254.6 (1.5%)  | 254.4 (1.4%)  | 255.1 (1.7%)  |
| 0.05        | 56.85                            | 61.17 (7.6%)  | 59.38 (4.5%)  | 57.04 (0.3%)  | 58.90 (3.6%)  |
| 0.25        | 13.35                            | 17.61 (32.0%) | 15.73 (17.8%) | 13.02 (-2.4%) | 15.14 (13.4%) |

The breakdown parameter is calculated using both the CFD and the DSMC solutions using Equation 2 with the derivative being taken in the direction of the steepest gradient. For this case of a cylinder in a hypersonic flow of a simple gas, the only causes of breakdown to the continuum hypothesis expected are in regions of high gradients (such as the shock and boundary layer) and regions of rarefaction (such as in the wake). The amount of continuum breakdown is also expected to increase as the gas flow becomes more rarefied. These trends are confirmed by the results that are shown below. In general, the flow experiences continuum breakdown in three areas; across the bow shock, in the boundary layer and in the wake region. The flow in the shock and boundary layer regions experiences very steep gradients in flow properties, while the wake region is more rarefied, thus leading to the breakdown of the continuum hypothesis.

In the results that follow, the surface properties are presented in terms of non-dimensionalized coefficients with the following definitions:

$$C_P = \frac{p - p_\infty}{\frac{1}{2}\rho_\infty U_\infty^2} \quad (16)$$

$$C_F = \frac{\tau}{\frac{1}{2}\rho_\infty U_\infty^2} \quad (17)$$

$$C_H = \frac{q}{\frac{1}{2}\rho_\infty U_\infty^3} \quad (18)$$

where  $p$  is the pressure,  $\tau$  is the shear stress,  $q$  is the heat transfer rate,  $p_\infty$  is the free stream pressure,  $\rho_\infty$  is the free stream density and  $U_\infty$  is the free stream velocity. The surface properties in each case are plotted as a function of the angle around the cylinder, with the stagnation point being located at an angle of zero (see Figure 1).



Table 4. Peak heat transfer rate.

Mach 10

| $Kn_\infty$ | Peak Heating [kW/m <sup>2</sup> ] (% Difference) |               |               |               |               |
|-------------|--------------------------------------------------|---------------|---------------|---------------|---------------|
|             | DSMC                                             | CFD (0)       | CFD (1)       | CFD (2)       | CFD (3)       |
| 0.002       | 89.80                                            | 89.85 (0.0%)  | 89.14 (-0.7%) | 89.00 (-0.9%) | 88.54 (-1.4%) |
| 0.01        | 39.13                                            | 40.22 (2.8%)  | 39.49 (0.9%)  | 39.20 (0.2%)  | 38.89 (-0.6%) |
| 0.05        | 15.92                                            | 18.08 (13.6%) | 17.25 (8.4%)  | 15.79 (-0.8%) | 16.81 (5.6%)  |
| 0.25        | 5.926                                            | 7.851 (32.5%) | 7.061 (19.1%) | 6.184 (4.3%)  | 6.640 (12.1%) |

Mach 25

| $Kn_\infty$ | Peak Heating [kW/m <sup>2</sup> ] (% Difference) |               |               |               |               |
|-------------|--------------------------------------------------|---------------|---------------|---------------|---------------|
|             | DSMC                                             | CFD (0)       | CFD (1)       | CFD (2)       | CFD (3)       |
| 0.002       | 1,746                                            | 1,763 (0.9%)  | 1,750 (0.2%)  | 1,746 (0.0%)  | 1,739 (-0.4%) |
| 0.01        | 749.6                                            | 791.0 (5.5%)  | 777.4 (3.7%)  | 768.4 (2.5%)  | 765.3 (2.1%)  |
| 0.05        | 309.9                                            | 357.9 (13.6%) | 341.0 (10.4%) | 294.2 (-4.8%) | 331.2 (7.2%)  |
| 0.25        | 105.7                                            | 147.8 (39.9%) | 133.6 (19.1%) | 111.7 (5.7%)  | 123.7 (17.0%) |

Along with the surface properties, the maximum  $Kn_{GLL}$  at the surface (based on the CFD solution with Type 2 slip conditions) is also plotted in each case.

IV.  $Kn = 0.002$

At a Knudsen number of 0.002, the flow is within the continuum, no-slip regime. Nevertheless, there is still evidence of continuum breakdown in the shock, along the cylinder surface in the boundary layer and in the wake as seen in Figure 4. Interestingly, DSMC predicts a larger degree of breakdown than does CFD. The increase in velocity from Mach 10 to Mach 25 also slightly increases the amount of breakdown predicted in the shock and wake regions.

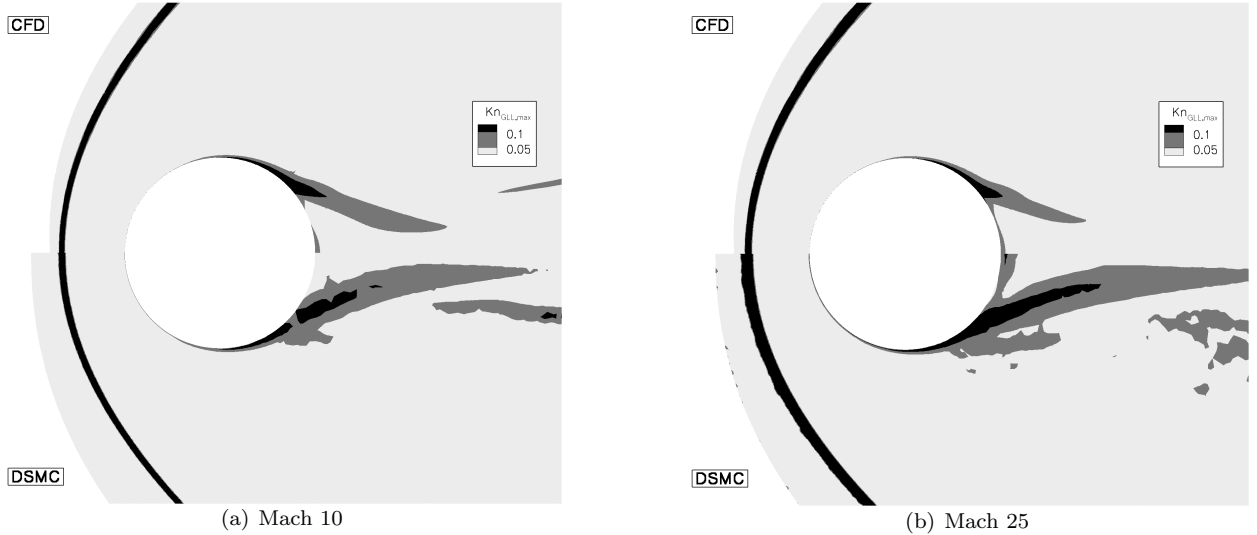


Figure 4.  $Kn_\infty = 0.002$   $Kn_{GLL}$  for Mach 10 and Mach 25. Light gray regions correspond to  $Kn_{GLL} < 0.05$ , dark gray regions correspond to  $0.05 < Kn_{GLL} < 0.10$  and black regions correspond to  $Kn_{GLL} > 0.10$ . Continuum breakdown is predicted in the shock region, in a thin boundary layer along the surface and in a region of flow expansion around the top of the cylinder.

The temperature field predicted by CFD and DSMC, as seen in Figure 5, is in excellent agreement, as expected. The Mach 25 case shows an increase in the maximum temperature as well as a slight increase in the shock thickness; however, for the presently considered simple gas, there are no other effects. The surface properties shown in Figures 6 - 8 show very good agreement between the two methods for all types of CFD boundary conditions considered, and for both Mach 10 and Mach 25. The only location along the surface where  $Kn_{GLL}$  is greater than 0.05 is in the wake region. The total drag and peak heat transfer rates predicted by the two methods differ by less than 1%, with only one exception (that being the Type 3 CFD solution at 1.4%). These results are well within the error range expected for a flow for which both methods are valid.

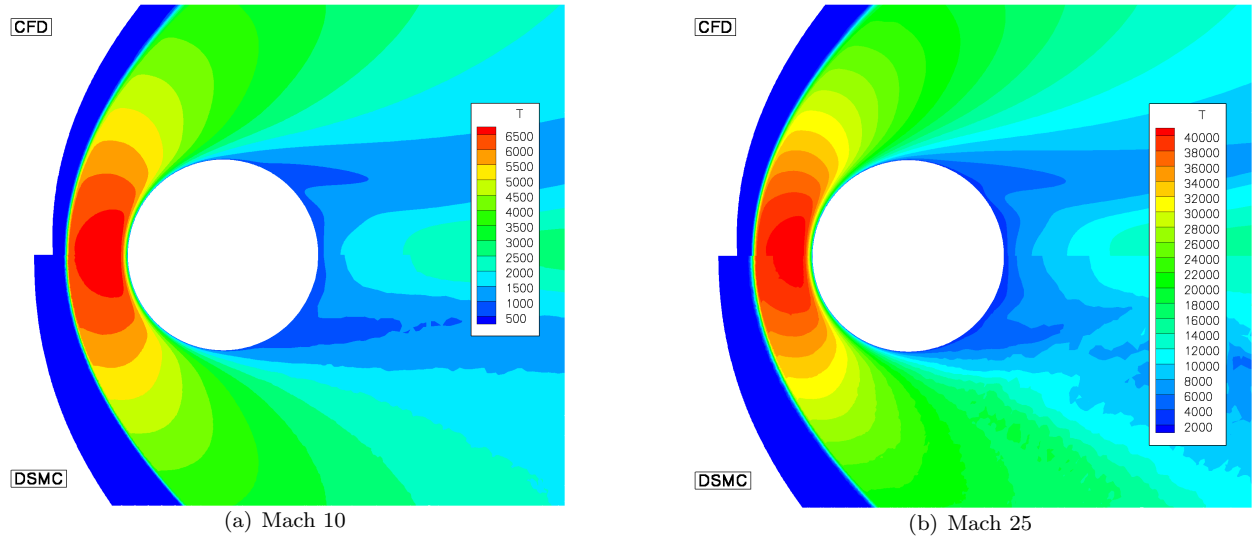


Figure 5.  $Kn_{\infty} = 0.002$  temperature field, for Mach 10 and Mach 25.

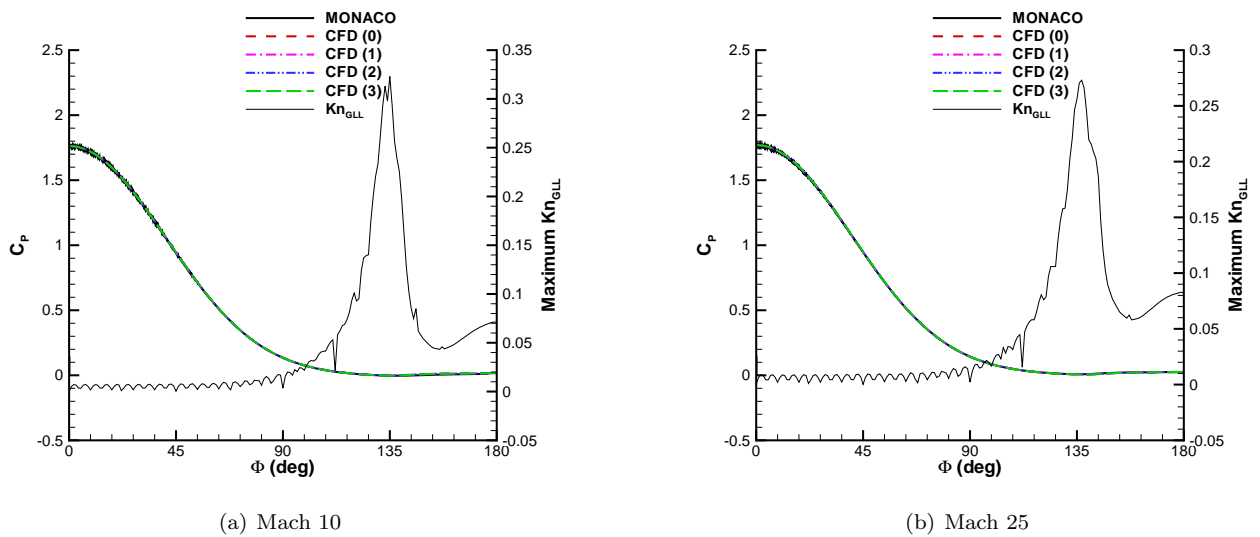
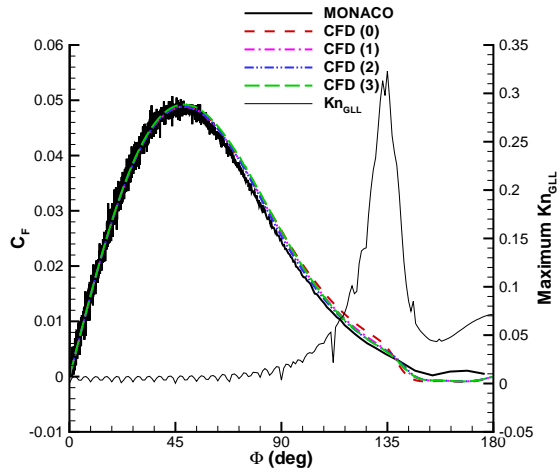
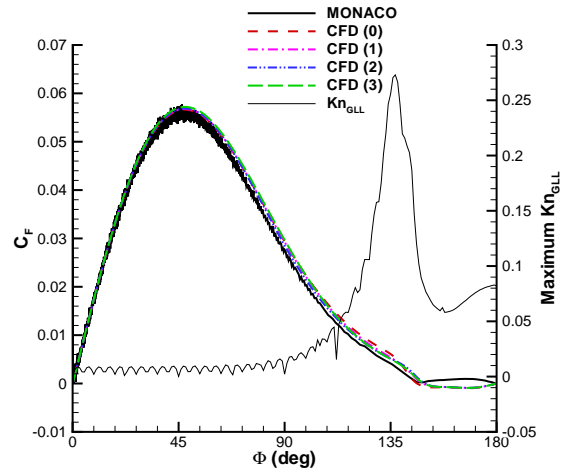


Figure 6.  $Kn_{\infty} = 0.002$  surface pressure coefficient and  $Kn_{GLL}$  for Mach 10 and Mach 25.

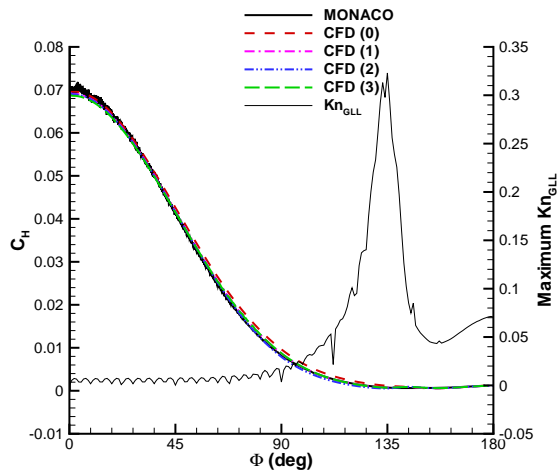


(a) Mach 10

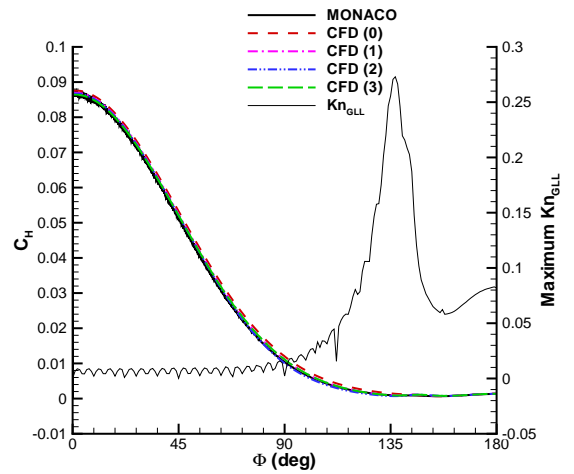


(b) Mach 25

Figure 7.  $Kn_\infty = 0.002$  surface friction coefficient and  $Kn_{GLL}$  for Mach 10 and Mach 25.



(a) Mach 10



(b) Mach 25

Figure 8.  $Kn_\infty = 0.002$  surface heating coefficient and  $Kn_{GLL}$  for Mach 10 and Mach 25.

## V. $Kn = 0.01$

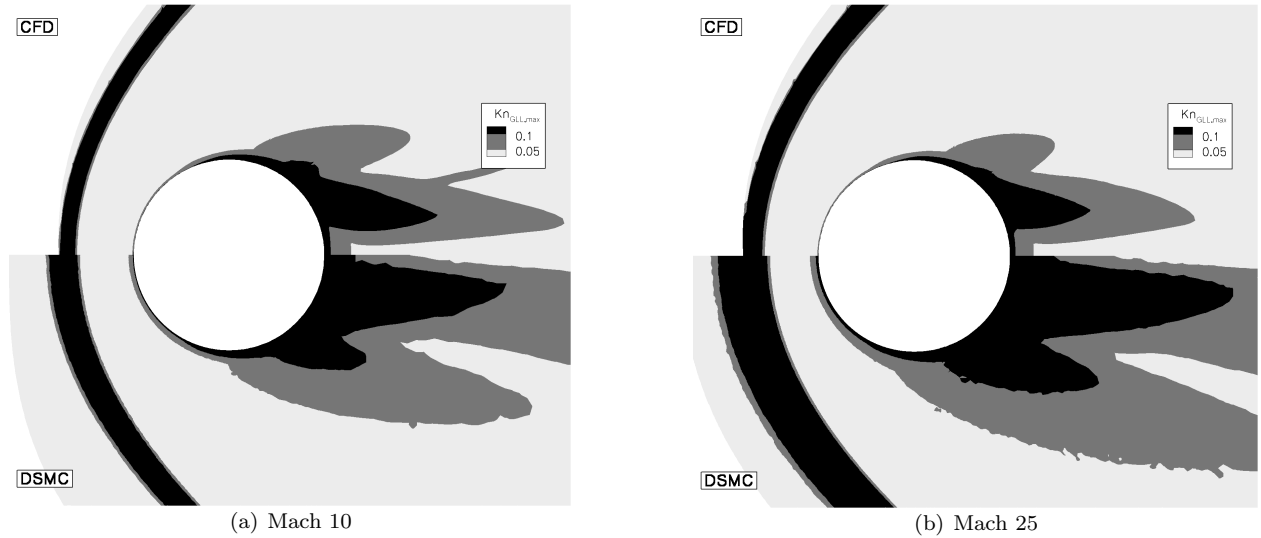


Figure 9.  $Kn_\infty = 0.01$   $Kn_{GLL}$  for Mach 10 and Mach 25. Light gray regions correspond to  $Kn_{GLL} < 0.05$ , dark gray regions correspond to  $Kn_{GLL} < 0.10$  and black regions correspond to  $Kn_{GLL} > 0.10$ . There are larger regions where continuum breakdown becomes a concern, especially in the wake, the shock and the boundary layer. The Mach 25 case shows larger regions than the Mach 10 case.

A Knudsen number of 0.01 is considered to be near the limit of the continuum, no-slip regime. Here there is increased evidence of continuum breakdown, as shown in Figure 9. However, comparison of general flow field features shows that the two numerical solutions (CFD and DSMC) do not differ much. The temperature field, seen in Figure 10, is very similar, with a few exceptions in the shock thickness and the wake (for Mach 25), where the continuum hypothesis is expected to break down first. The shock standoff distance predicted by both methods is nearly the same for the Mach 10 case, although there is more of a difference at Mach 25. The thicker shock does not seem to have an effect on the surface properties, as is shown below.

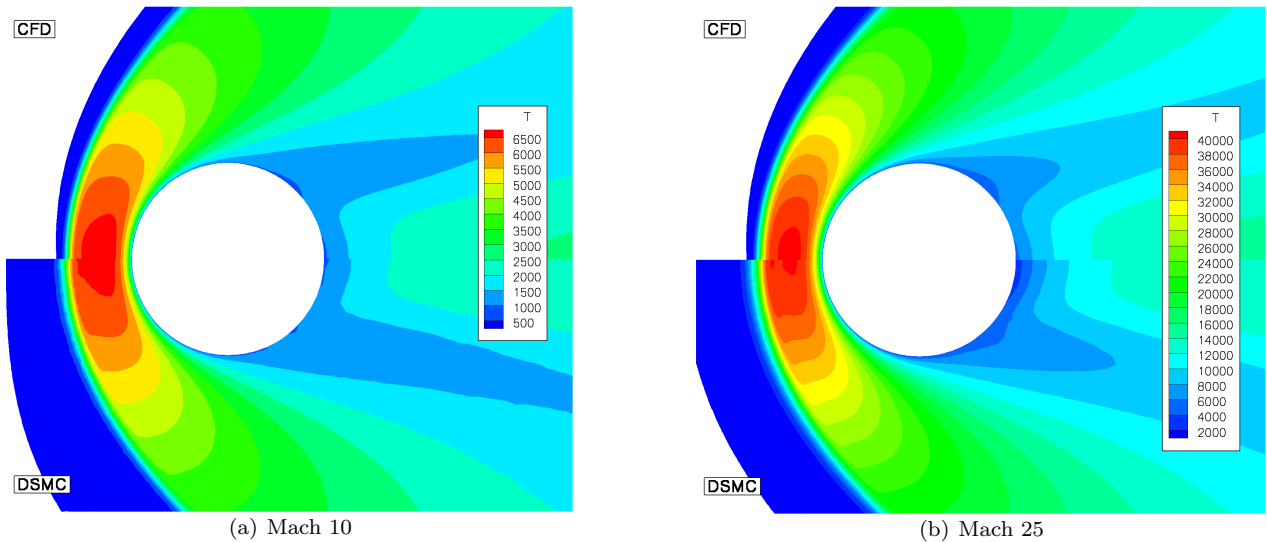


Figure 10.  $Kn_\infty = 0.01$  temperature field for Mach 10 and Mach 25.

The amount of breakdown in the shock does not necessarily carry over to the surface properties. Again, the amount of continuum breakdown near the surface does not seem to significantly affect the surface properties, shown in Figures 11 - 13. The no-slip CFD case (Type 0) shows some divergence from the others in the wake. The best agreement is achieved with the Type 2 and Type 3 slip conditions. Shear stress starts to diverge, even with the slip conditions, at Mach 25. This particular case seems to be somewhat of an aberration, especially when considering the good agreement that will be shown below for the  $Kn = 0.05$  case.

The heating rates also agree well at Mach 10, but show some differences at the higher velocities of Mach 25. The total drag due to pressure and viscous effects predicted by CFD is still within 1% of that predicted by DSMC, for Mach 10, and within 2% for Mach 25, as shown in Table 3. The peak heating also differs by less than 2% for the Mach 10 case when using slip boundary conditions, and less than 3% for the best slip conditions (Type 2 and Type 3) for the Mach 25 case. These results indicate that the surface properties are not strongly affected by the continuum breakdown in the shock, and the slip conditions improve the agreement quite satisfactorily.

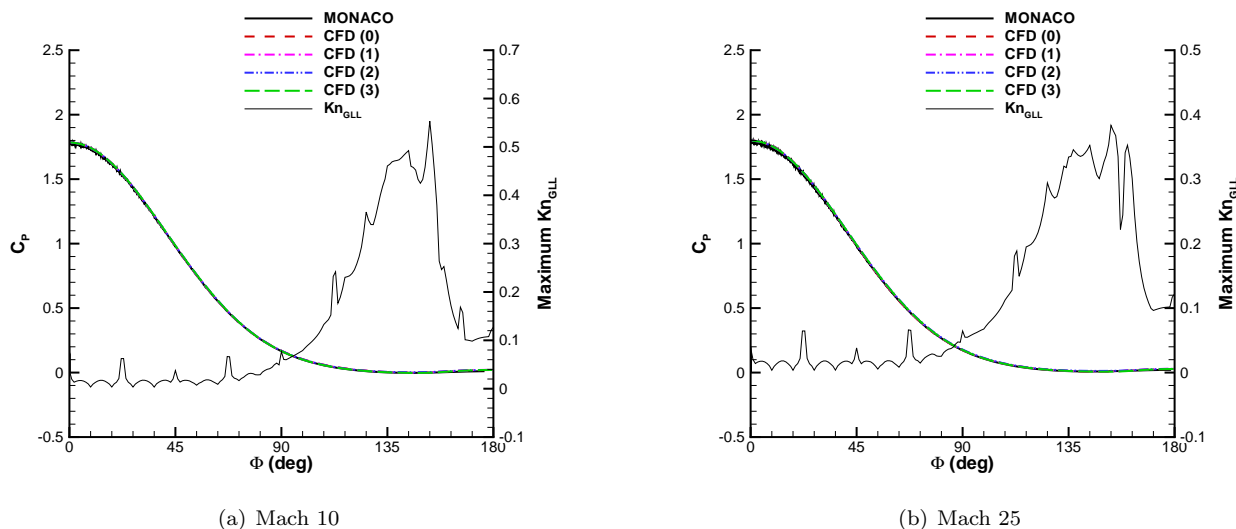


Figure 11.  $Kn_\infty = 0.01$  surface pressure coefficient and  $Kn_{GLL}$  for Mach 10 and Mach 25.

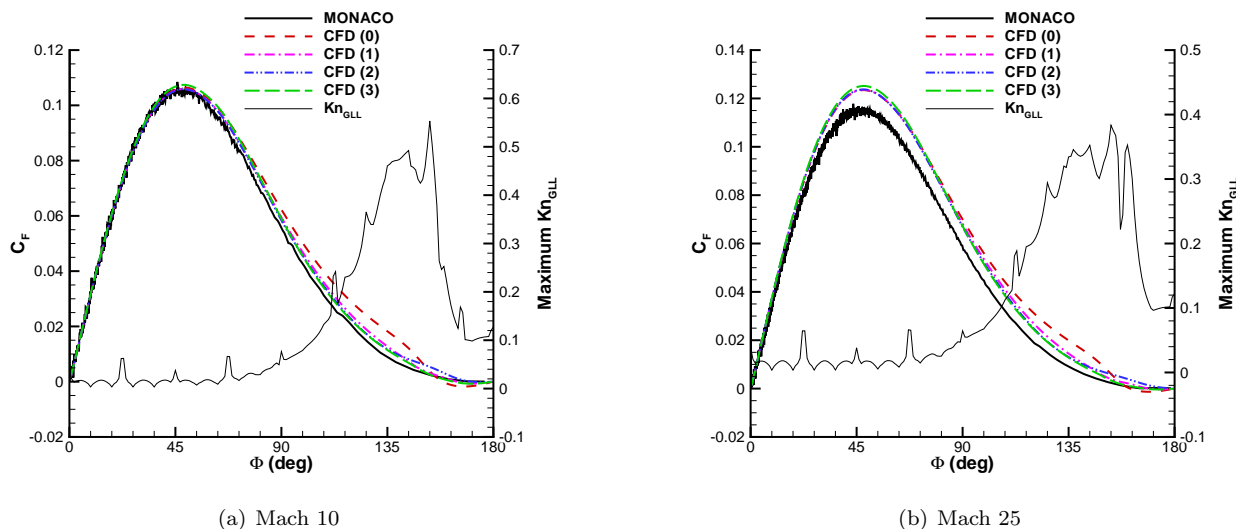
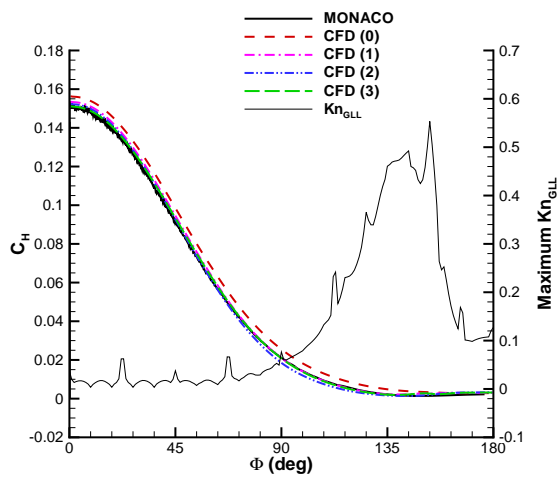
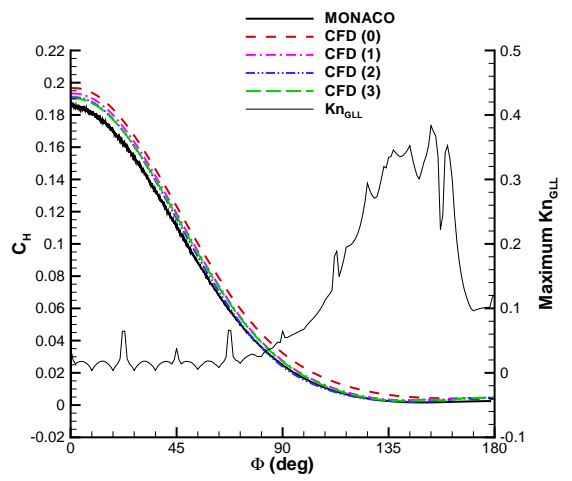


Figure 12.  $Kn_\infty = 0.01$  surface friction coefficient and  $Kn_{GLL}$  for Mach 10 and Mach 25.



(a) Mach 10



(b) Mach 25

Figure 13.  $Kn_\infty = 0.01$  surface heating coefficient and  $Kn_{GLL}$  for Mach 10 and Mach 25.

## VI. $Kn = 0.05$

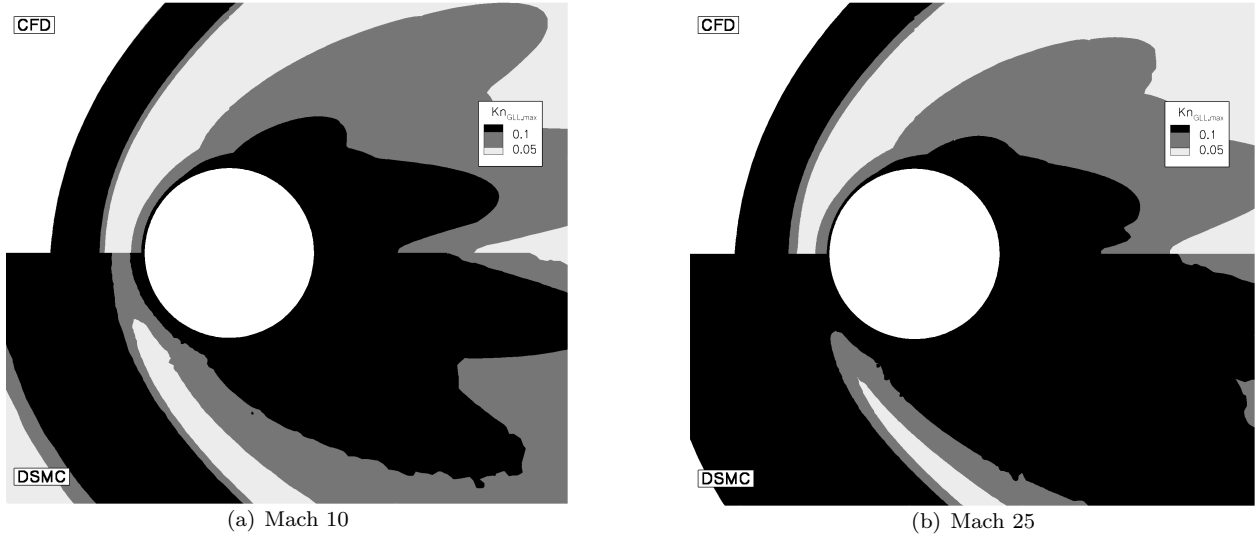


Figure 14.  $Kn_\infty = 0.05$   $Kn_{GLL}$  for Mach 10 and Mach 25. Light gray regions correspond to  $Kn_{GLL} < 0.05$ , dark gray regions correspond to  $Kn_{GLL} < 0.10$  and black regions correspond to  $Kn_{GLL} > 0.10$ . Continuum breakdown is predicted in much larger regions than previous cases. The DSMC method predicts larger regions where continuum breakdown exceeds the critical value of 0.05, with an even larger region predicted for the Mach 25 case. cylinder.

At a Knudsen number of 0.05, the flow is well within the slip regime. The flow demonstrates breakdown in a larger area of the flow, in each of the three regions (shock, boundary layer and wake), as seen in Figure 14. Again, there are larger areas in the Mach 25 case where the breakdown parameter exceeds the critical value of 0.05; in fact, nearly the entire domain is predicted to be beyond the region of applicability of the continuum equations. The differences between the CFD and DSMC temperature fields shown in Figure 15 are more pronounced than the lower Knudsen number cases, with even more differences for the higher Mach number case. The DSMC shock is much thicker than the CFD shock, although the shock stand-off distance and peak temperatures are still very nearly equal. In the wake, DSMC predicts a higher temperature than CFD.

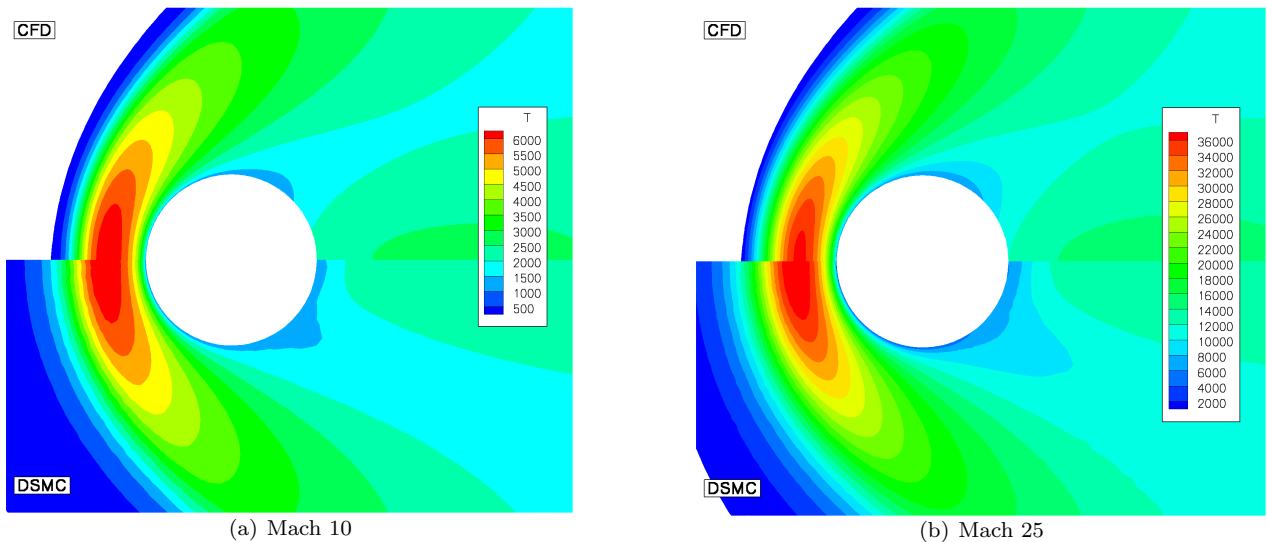


Figure 15.  $Kn_\infty = 0.05$  temperature field for Mach 10 and Mach 25.

The surface pressure predicted by both methods is still in excellent agreement, as seen in Figure 16. However, the shear stress is higher for most of the CFD cases, especially in the wake, with the surprising exception of the Type 2 case, which agrees almost exactly with the DSMC case (see Figure 17). The total drag for all of the slip cases are within 5% of the DSMC case, with the Type 2 case being almost identical.

The heat transfer rate, shown in Figure 18, also shows surprisingly good agreement between the Type 2 case and DSMC. While the no-slip case predicts a peak heat transfer rate about 13% higher than DSMC, the slip cases show better agreement, with the Type 2 case within 1% for Mach 10 and less than 5% for Mach 25.

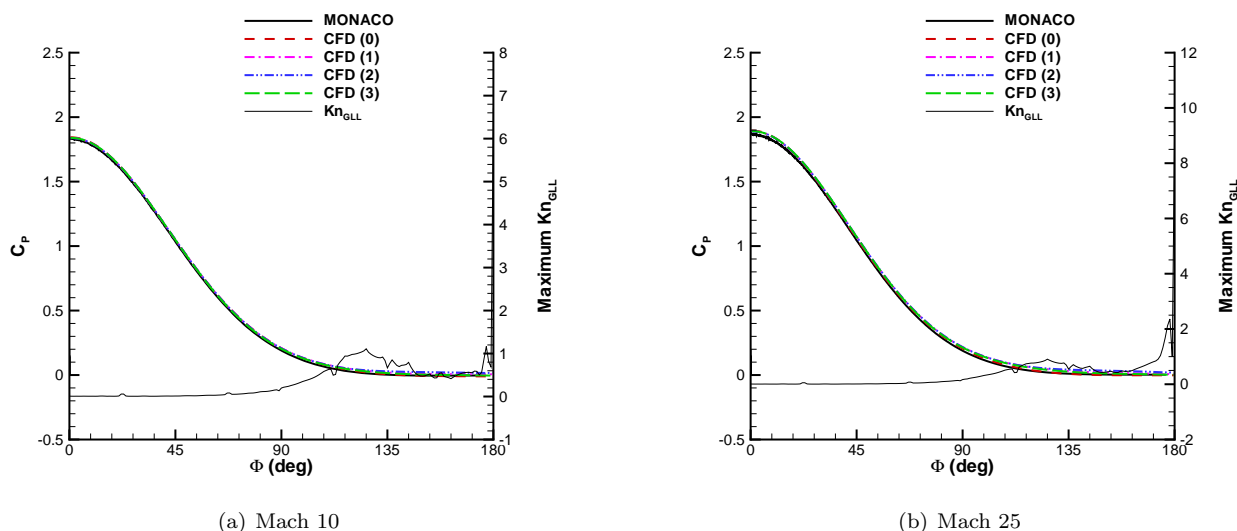


Figure 16.  $Kn_\infty = 0.05$  surface pressure coefficient and  $Kn_{GLL}$  for Mach 10 and Mach 25.

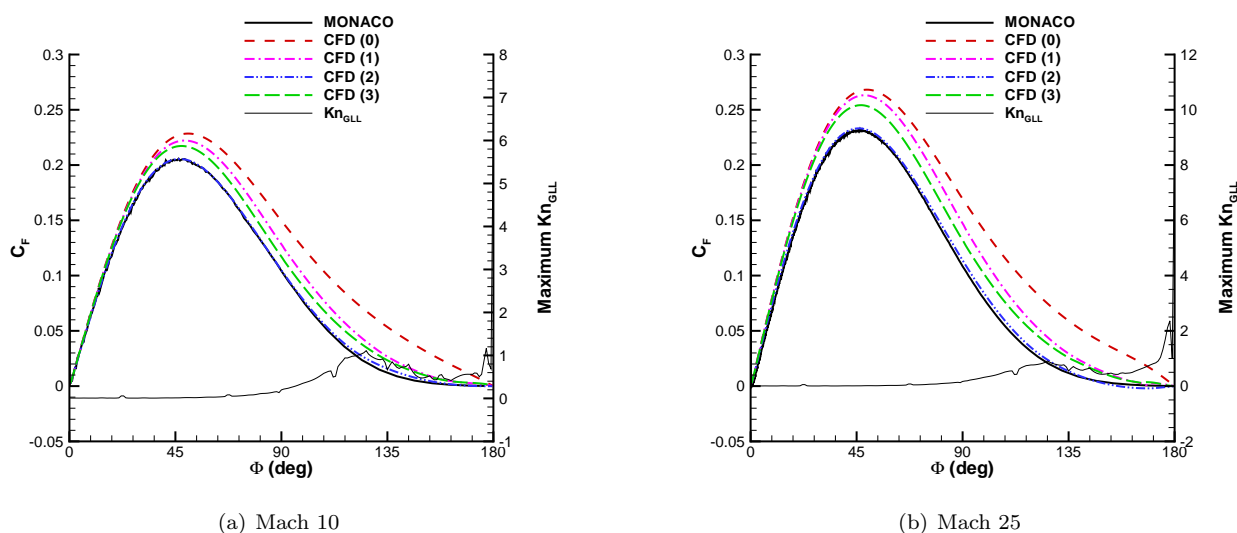
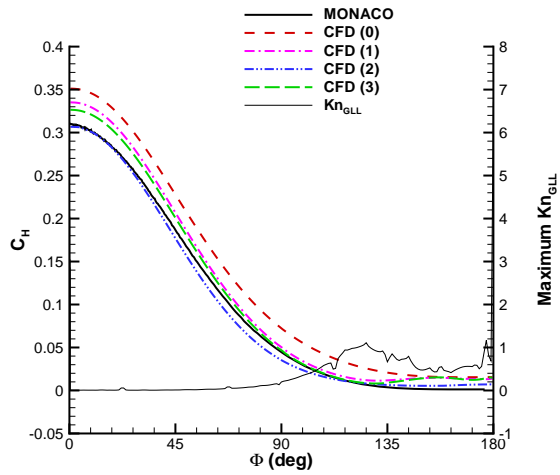


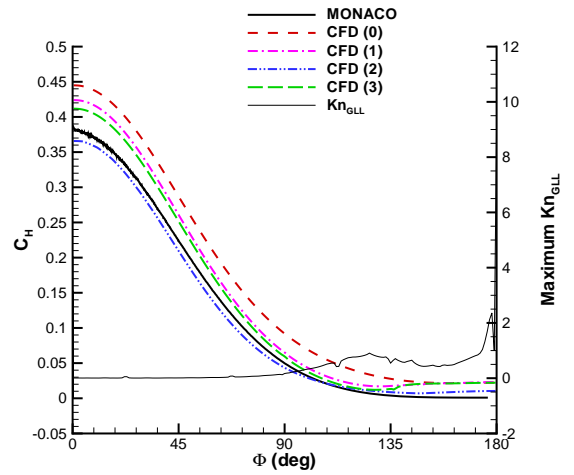
Figure 17.  $Kn_\infty = 0.05$  surface friction coefficient and  $Kn_{GLL}$  for Mach 10 and Mach 25.

The fortuitous agreement between the Type 2 CFD case and the DSMC case raises the question of how good the agreement is between flow properties, such as temperature and velocity, further from the surface. Recall that using the actual slip velocity and temperature jump as boundary conditions in a continuum method can improve wall properties such as shear stress and heat transfer, but may introduce additional errors in the predicted flow properties further from the wall. To investigate this possibility, the velocity and temperature (along with the breakdown parameter) are plotted along a line normal to the surface at an angle of  $90^\circ$ , and is shown in Figures 19 and 20. Both plots show that there is very good agreement between the CFD slip cases and the DSMC solution near the wall and extending out into the flow field for the Mach 10 case. For Mach 25, there is some disagreement in the temperature at the wall, although it recovers further out, while the agreement in velocity magnitude predicted is not as good. Therefore, there does not seem to be any concern about significant errors in flow properties predicted, at least in the case of the Mach 10 flow.



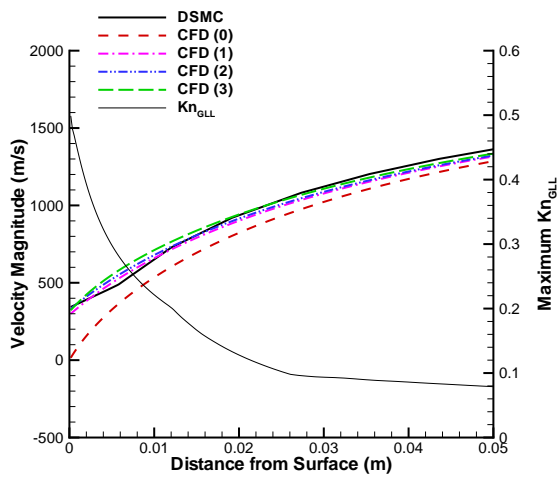


(a) Mach 10

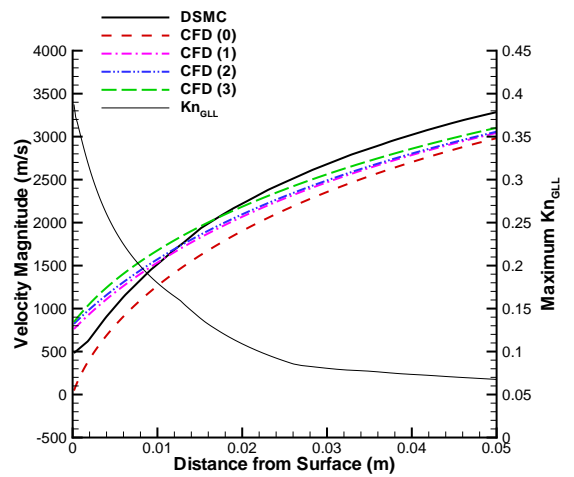


(b) Mach 25

Figure 18.  $Kn_\infty = 0.05$  surface heating coefficient and  $Kn_{GLL}$  for Mach 10 and Mach 25.



(a) Mach 10



(b) Mach 25

Figure 19.  $Kn_\infty = 0.05$  velocity magnitude and  $Kn_{GLL}$  along a line normal to body surface at  $\Phi = 90^\circ$ .

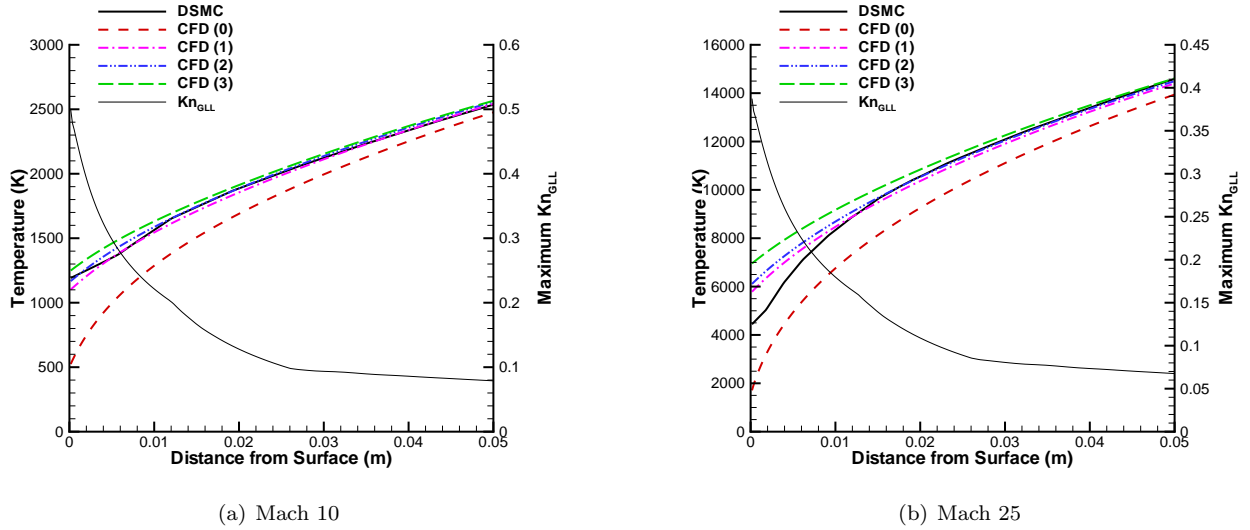


Figure 20.  $Kn_\infty = 0.05$  temperature and  $Kn_{GLL}$  along a line normal to body surface at  $\Phi = 90^\circ$ .

## VII. $Kn = 0.25$

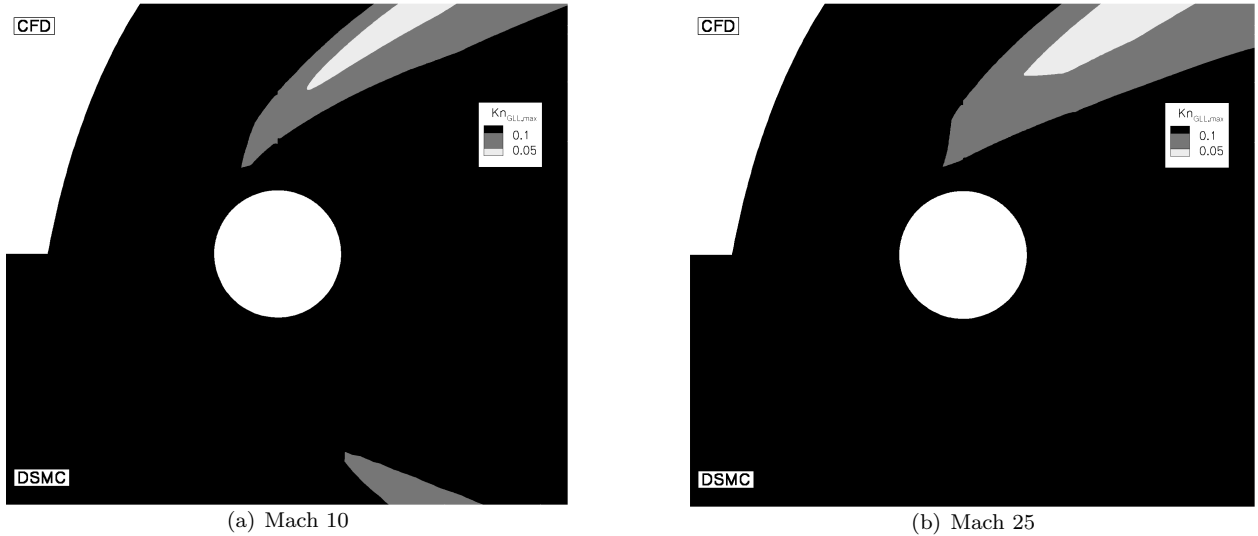


Figure 21.  $Kn = 0.25$   $Kn_{GLL}$  for Mach 10 and Mach 25. Light gray regions correspond to  $Kn_{GLL} < 0.05$ , dark gray regions correspond to  $Kn_{GLL} < 0.10$  and black regions correspond to  $Kn_{GLL} > 0.10$ . Continuum breakdown is predicted in almost the entire domain surrounding the cylinder.

For  $Kn_\infty = 0.25$ , the flow would be considered outside of the slip regime and into the transition regime. Here, even the addition of slip boundary conditions is not expected to help the continuum CFD method's predictive capabilities very much. Indeed, the plots of the breakdown parameter in Figure 21 indicate that there are significant non-equilibrium effects across almost all of the flow domain. The temperature fields predicted by both methods, seen in Figure 22, shows some major differences. Although the peak temperatures behind the shock appear to be about the same, the shock stand-off distances are significantly different, as is the thermal boundary layer thickness.

The surface pressure, plotted in Figure 23, predicted by both methods is also no longer in agreement, even for the CFD cases implementing slip conditions. The DSMC pressure is less than the CFD pressure near the fore-body (most likely due to the thinner shock predicted by CFD, which allows the CFD solution to approach the ideal jump condition more closely than the DSMC solution), but the agreement does improve in the wake. The pressure tensor at this Knudsen number is also most likely non-isotropic, which would

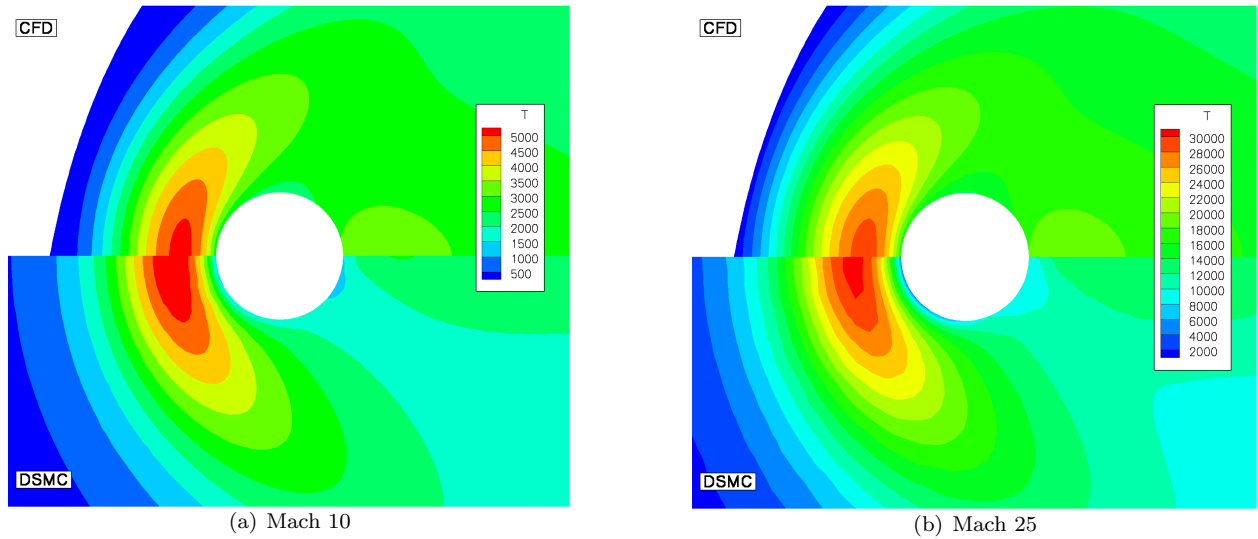


Figure 22.  $Kn = 0.25$  temperature field for Mach 10 and Mach 25.

introduce errors into the CFD solution. The shear stress, shown in Figure 24, shows the same general trend as in previous cases in that both methods agree near the stagnation region, but the results diverge as the flow accelerates around the cylinder. Here, the Type 2 CFD solution predicts a lower shear stress, but a higher pressure, thus the overall drag predictions are somewhat close (differing by about 5% for Mach 10 and less than 3% for Mach 25). The shear stress results also seem to indicate that the Type 2 CFD solution predicts some separation in the wake that is not predicted by the other models. The heat transfer rate, as seen in Figure 25, follows trends similar to the previous cases in that the DSMC heat transfer rate is lower than the CFD rate along the entire surface for all but the Type 2 case, which gets fairly close in some areas. The peak heat transfer rates differ by as much as almost 40% for the no-slip case at Mach 25, but the Type 2 case shows the best agreement with less than 5% difference at Mach 10 and less than 6% difference at Mach 25.

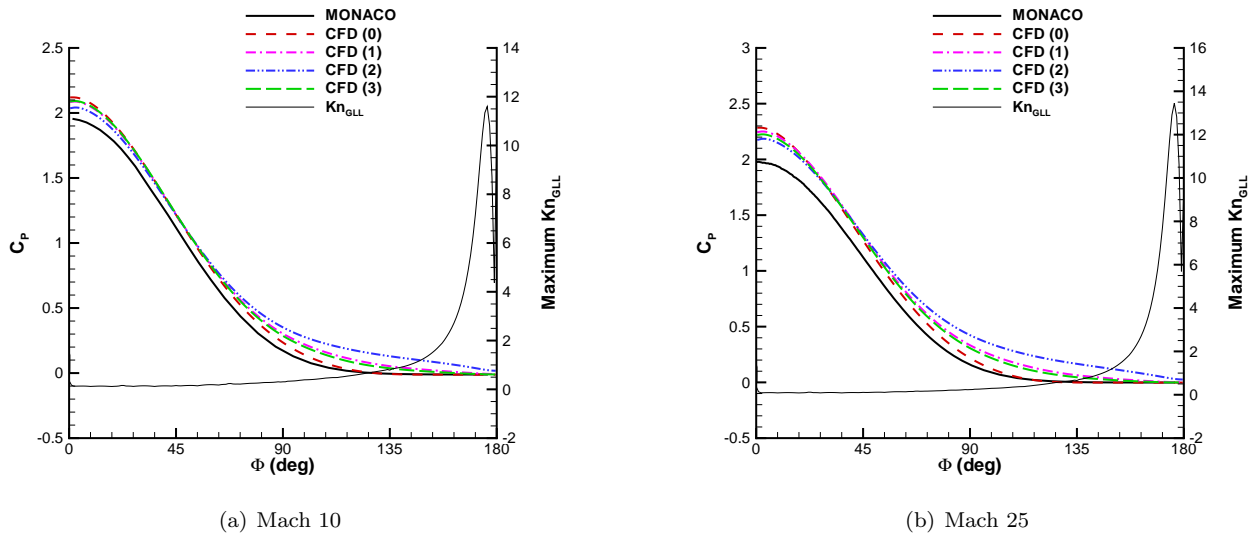
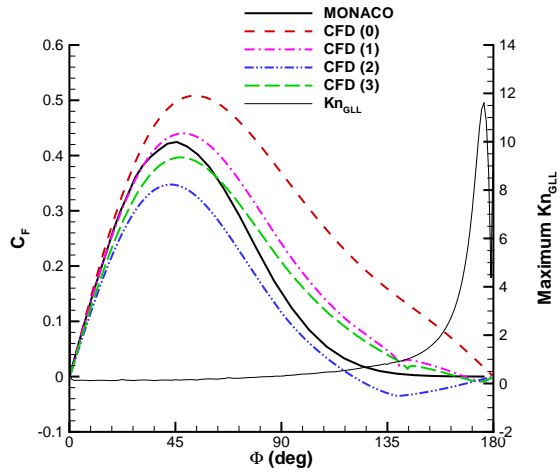
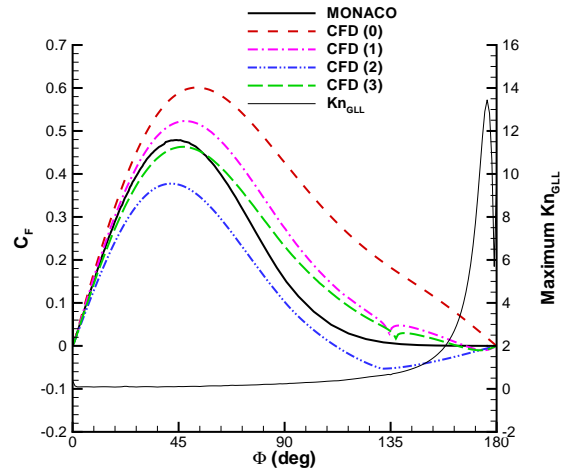


Figure 23.  $Kn_\infty = 0.25$  surface pressure coefficient and  $Kn_{GLL}$  for Mach 10 and Mach 25.

The velocity, temperature and breakdown parameter plotted along the line normal to the surface at an angle of  $90^\circ$  are shown in Figures 26 and 27. In this case, there are significant differences between the Type 2 case and DSMC, while the Type 1 and Type 3 cases show better agreement. It should be noted that the cells near the surface of the DSMC cases might not be small enough to capture the gradients in the Knudsen layer.

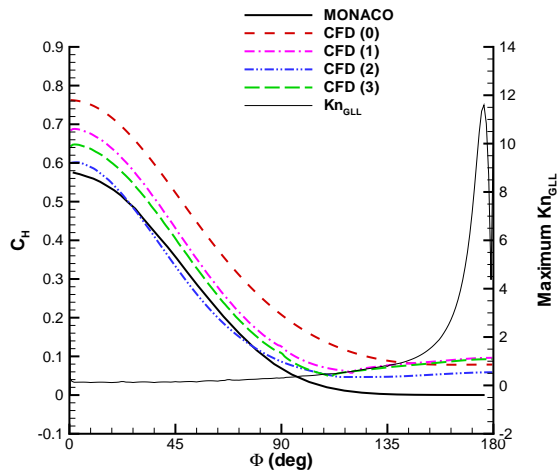


(a) Mach 10

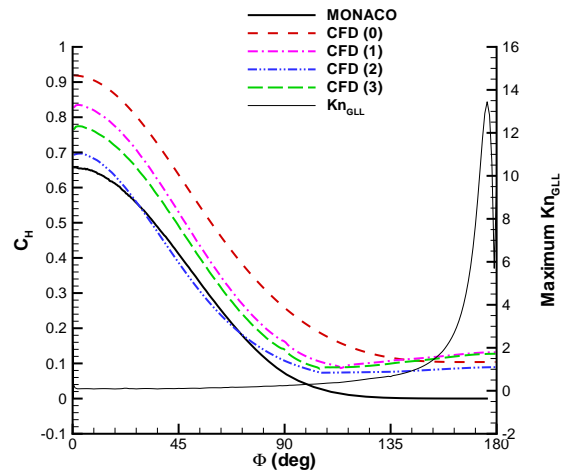


(b) Mach 25

Figure 24.  $Kn_\infty = 0.25$  surface friction coefficient and  $Kn_{GLL}$  for Mach 10 and Mach 25.

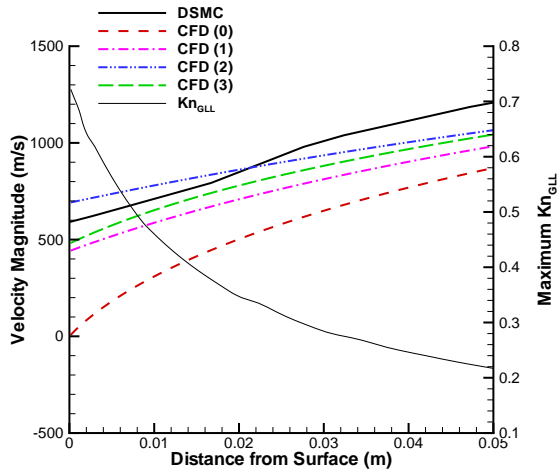


(a) Mach 10

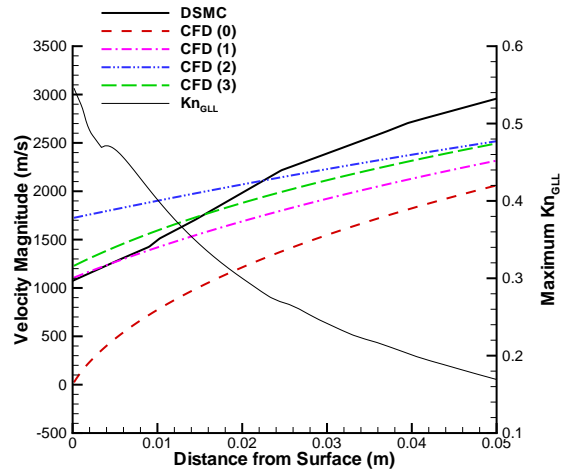


(b) Mach 25

Figure 25.  $Kn_\infty = 0.25$  surface heating coefficient and  $Kn_{GLL}$  for Mach 10 and Mach 25.

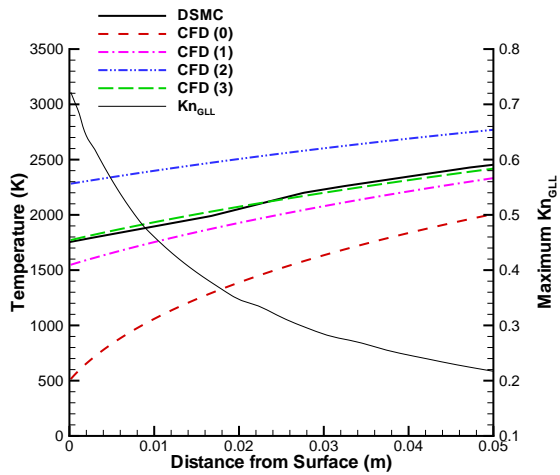


(a) Mach 10

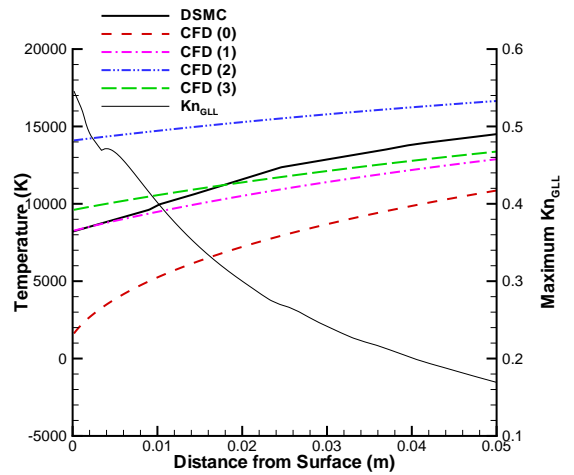


(b) Mach 25

Figure 26.  $Kn_\infty = 0.25$  velocity magnitude and  $Kn_{GLL}$  along a line normal to body surface at  $\Phi = 90^\circ$ .



(a) Mach 10



(b) Mach 25

Figure 27.  $Kn_\infty = 0.25$  temperature and  $Kn_{GLL}$  along a line normal to body surface at  $\Phi = 90^\circ$ .

## VIII. Conclusion

The primary goal of this study was to quantify the difference between DSMC and CFD simulations, when using slip boundary conditions, to determine the effects of different levels of continuum breakdown on surface properties under hypersonic flow conditions.

Comparison of CFD and DSMC results for identical flow conditions showed that the surface properties of pressure, shear stress and heat transfer rates were very similar for the lower Knudsen number flows where the continuum hypothesis is valid, as expected, while the results diverged in the higher Knudsen number cases. The surface pressure was least affected by continuum breakdown, as quantified by the gradient-length local Knudsen number, among those properties investigated, and seemed to be affected only by breakdown in the shock region at the highest Knudsen number flow. The shear stress was most influenced by continuum breakdown and was affected primarily by continuum breakdown in the wake. The addition of slip velocity and temperature jump boundary conditions greatly improved the agreement at higher Knudsen numbers. Several different types of slip boundary conditions were examined, and the best agreement appears to be obtained when using the generalized slip conditions proposed by Gökçen. With these boundary conditions, the difference in surface properties predicted by CFD and DSMC increased from less than 1% at  $Kn_\infty = 0.002$  to around 5% at  $Kn_\infty = 0.25$ .

For the case of a simple gas, the higher velocities associated with a Mach 25 flow did not seem to increase the difference between the CFD and DSMC predictions. Although the extent of the region where the continuum breakdown parameter exceeded the critical value of 0.05 was larger at the higher Mach number, the predicted surface properties with the slip boundary conditions still remained well under 5% for all but the  $Kn_\infty = 0.25$  case, where the peak heat transfer rates and total drag predictions were within 6%.

## Future Work

The present case was limited to a simple gas. Gases comprised of diatomic molecules, such as nitrogen, are expected to present additional difficulties, such as vibrational relaxation and dissociation rates, especially for the higher temperatures encountered at Mach 25.

Additionally, different geometries, such as sharp leading edges with attached shocks, are expected to present more challenges in getting CFD predictions to agree with those from DSMC due to the highly non-equilibrium behavior near the leading edge.

## Acknowledgments

The first author gratefully acknowledges the support of the Air Force Institute of Technology. This work is also sponsored in part by the Space Vehicle Technology Institute, under NASA grant NCC3-989 with joint sponsorship from the Department of Defense, and by the Air Force Office of Scientific Research, through grant FA9550-05-1-0115. The generous use of NASA high performance computing resources was indispensable to this investigation and is greatly appreciated.

## References

- <sup>1</sup>Bird, G. A., *Gas Dynamics and the Direct Simulation of Gas Flows*, Oxford University Press, Oxford, 1994.
- <sup>2</sup>Bird, G. A., "Breakdown of Translational and Rotational Equilibrium in Gaseous Expansions," *AIAA Journal*, Vol. 8, No. 11, 1970, pp. 1998–2003.
- <sup>3</sup>Tiwari, S., "Coupling of the Boltzmann and Euler Equations with Automatic Domain Decomposition," *Journal of Computational Physics*, Vol. 144, Aug. 1998, pp. 710–726.
- <sup>4</sup>Garcia, A. L., Bell, J. B., Crutchfield, W. Y., and Alder, B. J., "Adaptive Mesh and Algorithm Refinement Using Direct Simulation Monte Carlo," *Journal of Computational Physics*, Vol. 154, 1999, pp. 134.
- <sup>5</sup>Camberos, J. A., Schrock, C. R., McMullan, R. J., and Branam, R. D., "Development of Continuum Onset Criteria with Direct Simulation Monte-Carlo Using Boltzmann's H-Theorem: Review and Vision," *Proceedings of the 9th AIAA/ASME Joint Thermophysics and Heat Transfer Conference*, San Francisco, California, June 2006.
- <sup>6</sup>Boyd, I. D., Chen, G., and Candler, G. V., "Predicting Failure of the Continuum Fluid Equations in Transitional Hypersonic Flows," *Physics of Fluids*, Vol. 7, No. 1, Jan. 1995, pp. 210–219.
- <sup>7</sup>Wang, W.-L., *A Hybrid Particle/Continuum Approach for Nonequilibrium Hypersonic Flows*, Phd thesis, The University of Michigan, 2004.
- <sup>8</sup>Lofthouse, A. J., Boyd, I. D., and Wright, M. J., "Effects of Continuum Breakdown on Hypersonic Aerothermodynamics," *AIAA Paper 2006-0993*, presented at the 44th AIAA Aerospace Sciences Meeting and Exhibit, Reno, NV, Jan. 2006.

- <sup>9</sup>Scalabrin, L. C. and Boyd, I. D., “Development of an Unstructured Navier-Stokes Solver for Hypersonic Nonequilibrium Aerothermodynamics,” *AIAA Paper 2005-5203*, presented at the 38th AIAA Thermophysics Conference, Toronto, Ontario Canada, June 2005.
- <sup>10</sup>Scalabrin, L. C. and Boyd, I. D., “Numerical Simulation of Weakly Ionized Hypersonic Flow for Reentry Configurations,” *AIAA Paper 2006-3773*, presented at the 9th AIAA/ASME Joint Thermophysics and Heat Transfer Conference, San Francisco, CA, June 2006.
- <sup>11</sup>Dietrich, S. and Boyd, I. D., “Scalar and Parallel Optimized Implementation of the Direct Simulation Monte Carlo Method,” *Journal of Computational Physics*, Vol. 126, No. 2, 1996, pp. 328–342.
- <sup>12</sup>Sun, Q., Cai, C., Boyd, I. D., Clemmons, J. H., and Hecht, J. H., “Computational Analysis of High-Altitude Ionization Gauge Flight Measurements,” *Journal of Spacecraft and Rockets*, Vol. 43, No. 1, 2006, pp. 186–193.
- <sup>13</sup>Schwartzentruber, T. E., Scalabrin, L. C., and Boyd, I. D., “Hybrid Particle-Continuum Simulations of Non-Equilibrium Hypersonic Blunt Body Flow Fields,” *AIAA Paper 2006-3602*, presented at the 9th AIAA/ASME Joint Thermophysics and Heat Transfer Conference, San Francisco, CA, June 2006.
- <sup>14</sup>Bird, G. A., “Sophisticated Versus Simple DSMC,” *Rarefied Gas Dynamics: 25th Symposium on Rarefied Gas Dynamics*, AIP Conference Proceedings, St. Petersburg, Russia, 2006.
- <sup>15</sup>Lockerby, D. A., Reese, J. M., Emerson, D. R., and Barber, R. W., “Velocity boundary condition at solid walls in rarefied gas calculations,” *Physical Review E*, Vol. 70, No. 017303, 2004.
- <sup>16</sup>Gökçen, T. and MacCormack, R. W., “Nonequilibrium Effects for Hypersonic Transitional Flows Using Continuum Approach,” *AIAA Paper 1989-0461*, presented at the 27th Aerospace Sciences Meeting, Reno, NV, Jan. 1989.
- <sup>17</sup>Gökçen, T., MacCormack, R. W., and Chapman, D. R., “Computational Fluid Dynamics Near the Continuum Limit,” *AIAA Paper 1987-1115*, 1987.
- <sup>18</sup>Sharipov, F. and Kamekura, D., “Velocity slip and temperature jump coefficients for gaseous mixtures. I. Viscous slip coefficient,” *Physics of Fluids*, Vol. 15, No. 6, June 2003, pp. 1800–1806.
- <sup>19</sup>Street, R. E., “A Study of Boundary Conditions in Slip-Flow Aerodynamics,” *Rarefied Gas Dynamics, Proceedings of the First International Symposium held at Nice*, edited by F. M. Devienne, Pergamon Press, New York, 1960, pp. 276–292.
- <sup>20</sup>Lockerby, D. A., Reese, J. M., and Gallis, M. A., “Capturing the Knudsen Layer in Continuum-Fluid Models of Nonequilibrium Gas Flows,” *AIAA Journal*, Vol. 43, No. 6, June 2005, pp. 1391–1393.
- <sup>21</sup>Bird, G. A., “The DS2V/3V Program Suite for DSMC Calculations,” *Rarefied Gas Dynamics*, edited by M. Capitelli, AIP Conference Proceedings 762, New York, 2000, pp. 541–546.
- <sup>22</sup>Bird, G. A., private communication, Sept. 2006.
- <sup>23</sup>McNenly, M. J., Gallis, M. A., and Boyd, I. D., “Empirical slip and viscosity model performance for microscale gas flow,” *International Journal for Numerical Methods in Fluids*, Vol. 49, No. 11, Sept. 2005, pp. 1169–1191.
- <sup>24</sup>Bayazitoglu, Y. and Tunc, G., “Extended slip boundary conditions for microscale heat transfer,” *Journal of Thermophysics and Heat Transfer*, Vol. 16, No. 3, 2002, pp. 472–475.